# One-body theory for amplified signal response in a scale-free network

Takeo Kondo,[1] Zonghua Liu,[2] and Toyonori Munakata[1]
[1]*Department of Applied Mathematics and Physics, Graduate School of Informatics, Kyoto University, Kyoto 606-8501, Japan*
[2]*Institute of Theoretical Physics, East China Normal University, Shanghai 200062, China*
(Received 31 August 2009; revised manuscript received 27 November 2009; published 15 April 2010)

It has recently been shown that amplified signal response is possible in scale-free networks of two-state signaling devices [J. A. Acebron *et al.*, Phys. Rev. Lett. **99**, 128701 (2007)]. In the analysis of dynamics in networks, much emphasis is put on the hub, and consequently the applicability thereof is limited to a region of small coupling strength. In this paper, we develop a one-body theory which predicts (1) the behavior of the gain in the whole coupling strength region, and (2) the degree of the unit, which shows maximum response, as a function of the coupling strength. In order to achieve good agreement with numerical experiments effects of finite system size are taken into account when the coupling strength becomes very small and the degree $k_L$ of the maximum response unit, predicted by our theory, becomes larger than the maximum degree $k_{max}$ available to a concrete finite network.

DOI: 10.1103/PhysRevE.81.041115 PACS number(s): 05.40.−a, 05.45.Xt, 89.75.Hc

## I. INTRODUCTION

A bistable unit has long been employed mainly to describe physical and chemical systems/processes, such as glasses [1] and chemical reactions [2]. However, it is now gathering considerable interest as an information processing unit and is used as a paradigm of stochastic resonance (SR), which was first formulated for a system with double well potential [3] and represents an interesting phenomenon, in which detectability of a weak input signal is enhanced by the assistance of proper amount of noise [4].

Much effort has been naturally invested to study effects of coupling many bistable units on the detectability [4]. One new aspect here is that we have an extra parameter of coupling strength and the detectability turned out to achieve maximum at a finite coupling strength in some networks with array [5], and scale-free [6] connections. Thus, we may have a kind of double resonance with respect to noise strength (as in SR) and the coupling strength [5,6].

Recently, Acebron *et al.* [7] investigated a scale-free (SF) network with a double well unit put on each node, from a viewpoint of signal detection via complex network topology, which may be a kind of sources of diversity [8]. The gain, $G$, which quantifies detectability of the input sinusoidal signal, was shown by computer simulations to have a plateau in some range of the coupling strength $\lambda$. Theoretically they analyzed collective dynamics in the highly heterogeneous network by proposing a simplified starlike model, in which a hub unit (i.e., star) was connected with many other units (i.e., leaves) isolated from all other units.

Although they could show that the existence of the hub unit played the decisive role to make the gain large, their theory is limited to a region of small coupling strength. As a result, properties of the scale-free network seems to be not fully elucidated, and the roles of network structures such as the power-law degree distribution in the scale-free network [8] remains to be clarified. In this paper, we develop a one-body theory, which enables us to give analytic expressions not only for the gain $G$ but also for the degree $k_L$ of the unit with the maximum response to the input signal in terms of the coupling strength $\lambda$.

When $\lambda$ approaches zero, the degree $k_L$ with the maximum response goes to infinity and we have taken into account effects of finite system size to explain our simulation results. On the other hand as $\lambda$ becomes large, the system shows full synchronization to a input periodic signal, which is also analyzed based on a one-body theory.

The paper is organized as follows. Section II gives the one-body theory and its approximation conditions. Section III discusses the gain for the whole coupling range and shows its consistence with numerical simulations. Finally, Sec. IV includes the discussion and the conclusions.

## II. ONE-BODY THEORY

The model we study is described by [7]

$$\dot{x}_i = -dV(x_i)/dx_i + A\sin(\omega t) + \lambda\sum_{j=1}^{N} M_{ij}(x_j - x_i), \qquad (1)$$

where $x_i (i=1,\ldots,N)$ denotes the response of the unit $i$ to the sinusoidal input signal and $\lambda(>0)$ is the coupling strength. We will choose $V(x)$ as a double well potential, which takes the form [6]

$$V(x) = (x-1)^2(x+1)^2. \qquad (2)$$

$M$ is the adjacency matrix. That is, $M_{ij}=1$ if there is coupling between the unit $i$ and $j$ and $M_{ij}=0$ otherwise. We will mainly consider a scale-free network with the average degree $\langle k\rangle=6$, which is produced by a Barabasi-Albert algorithm [9]. The scale-free network has the degree distribution

$$P(k) \propto k^{-3}. \qquad (3)$$

Under the action of the sinusoidal signal, each oscillator $x_i$ performs a periodic motion in a stationary state with the amplitude defined by $a_i \equiv [\max_t x_i(t) - \min_t x_i(t)]/2$. The gain $G$, which measures efficiency for information processing, is defined by [7]

 

$$G \equiv \max_i a_i/A \equiv a_L/A, \tag{4}$$

where the unit $L$ denotes the one with the maximum amplitude. As for the initial condition $\{x_i(t=0)\}(i=1,2,\ldots,N)$ we will follow [7], in which $x_i(t=0)$ is chosen to be either 1 or $-1$ with the probability 1/2.

Let us first introduce the concept of a *fifty-fifty* unit. If a unit $i$ belongs to the fifty-fifty unit, this means that about half of its neighbors $(k_i/2)$ are oscillating in the left well $(x \simeq -1)$ and the other half in the right well $(x \simeq 1)$ in a stationary state, and we express this as $i \in F$. The key observation, which enabled us to reduce Eq. (1) to a one-body problem for $G$, is that the unit $L$, which realizes maximum response $a_L$, belongs to the fifty-fifty unit, i.e., $L \in F$. This is first occurred to us through data analysis of our numerical experiments and later turned out to be reasonable.

If $i \in F$ and is located on the left well at some time, the unit $i$ feels attractive force from $k_i/2$ units in the right well with nearly no force from $k_i/2$ units in the left well. If the force happens to be strong enough to pull the unit $i$ to the right well over the potential barrier of $V(x)$, it moves to the right well and a similar event occurs to bring back the unit $i$ to the left well. This is a mechanism for a unit to perform large amplitude oscillation around the center $x=0$.

This is easily formulated with use of Eq. (1) as follows: If we choose arbitrarily a unit $i \in F$, to be called $f$ for convenience, we can write down Eq. (1) as

$$\dot{x}_f = -4x_f^3 + (4 - \lambda k_f)x_f + A\,\sin(\omega t) \equiv -dV_{eff}(x_f)/dx_f + A\,\sin(\omega t), \tag{5}$$

where the assumption $\Sigma_j M_{fj} x_j \ll \Sigma_j M_{fj} x_f = k_f x_f$ is used. In a stationary state $x_f(t)$ performs a periodic oscillation with the period $\tau_p \equiv 2\pi/\omega$ and we denote the solution as $x_{f,p}(t)$. As will be shown below its amplitude shows interesting bifurcation as a function of $\lambda k_f$ with the critical point at $\lambda k_f^c = 1.721$.

In Fig. 1 we show four trajectories $x_{f,p}(t)$ for $\lambda k_f = 1$, 1.72, 1.722, and 4, which are obtained by solving Eq. (5) numerically by a Runge-Kutta method [10]. When $\lambda k_f$ is small, Fig. 1(a), we have two solutions, one oscillating around 1 and the other around $-1$ (not shown).When $\lambda k_f$ is large, Fig. 1(d), the periodic oscillation is around $x=0$. At the subcritical point, Fig. 1(b), the unit performs strongly nonlinear oscillation in the regions $1 > x > 0$ and $0 > x > -1$ (not shown). On the other hand the unit oscillates around $x=0$ with large amplitude at the postcritical point, Fig. 1(c), thus showing a bifurcation of oscillation amplitude at $\lambda k_f^c = 1.721$.

In Fig. 2, we plot $Z(\lambda k_f) \equiv \max_t x_f(t) - \min_t x_f(t) \equiv X_{f,max} - X_{f,min}$ as a function of $\lambda k_f$ (the solid curve). Around $\lambda k_f^c \simeq 1.721$ we observe a jump of $Z(\lambda k_f)$.

As preparation for our analytic theory to be developed later, let us study this bifurcation graphically from a little different viewpoint, which results in confirmation of the bifurcation picture obtained above from Fig. 1. For the purpose we introduce $A_{max}$ $(A_{min})$ as the value of $A\,\sin(\omega t)$, when $x_{f,p}(t)$ takes its maximum $X_{f,max}$(minimum $X_{f,min}$), which can be read off easily from Fig. 1.

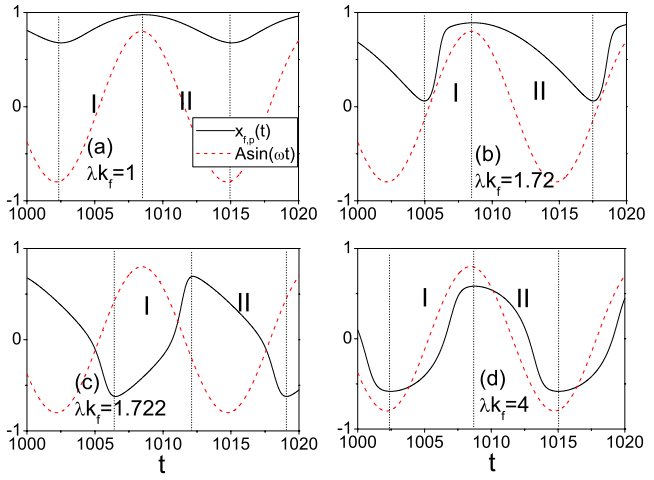


FIG. 1. (Color online) Periodic solution $x_{f,p}(t)$ of Eq. (5) for (a) $\lambda k_f = 1$, (b) 1.72, (c) 1.722, and (d) 4 for $A=0.8$ and $\omega=0.5$ (solid curves). The periodic external force $A\,\sin(\omega t)$ is also shown as dashed curves. The vertical dotted lines represent the points where $x_{f,p}(t)$ become maximum and minimum. In the region I (II) $x_{f,p}(t)$ increases (decreases).

The pair $(X_{f,max}, A_{max})$ is easily seen to satisfy the following algebraic equation,

$$g(X_{f,max}) \equiv -dV_{eff}(X_{f,max})/dX_{f,max} = -A_{max}, \tag{6}$$

with the same equation holding for the pair $(X_{f,min}, A_{min})$ also.

In Fig. 3 we plot $A_{max}$ and $A_{min}$ as a function of $\lambda k_f$. At this point we give two remarks on the periodic solution $x_{f,p}(t)$, which are useful for discussing the bifurcation. The first one is that if $x_{f,p}(t)$ is a periodic solution of Eq. (5) with $A_{max}$ and $A_{min}$, then $x'_{f,p}(t) \equiv -x_{f,p}(t + \pi/\omega)$ is also a solution of Eq. (5) with $A'_{max} = -A_{min}$ and $A'_{min} = -A_{max}$. The second one is that if $g(X)=B$, with $B$ a constant, has three solutions $X_1 < X_2 < X_3$, then $g(X)=-B$ has three solutions $-X_3 < -X_2 < -X_1$. When there is only one real solution $X_1$ to $g(X)=B$, then $g(X)=-B$ has $-X_1$ as its solution.

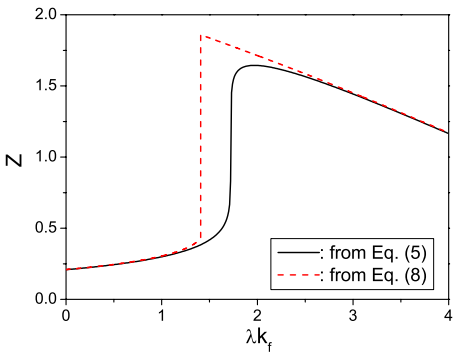


FIG. 2. (Color online) $Z$ versus $\lambda k_f$ for $A=0.8$ and $\omega=0.5$, where the solid curve comes from the periodic (numerical) solution $x_{f,p}$ to Eq. (5) and the dashed curve is from the solution of Eq. (8), which results from Eq. (5) after introducing additional approximation Eq. (7).

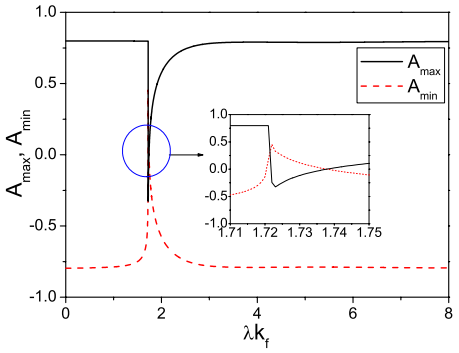


FIG. 3. (Color online) $A_{max}$ (solid curve) and $A_{min}$ (dashed curve) versus $\lambda k_f$ for $A=0.8$. The approximation $A_{max}(\lambda k_f)=0.8$ and $A_{min}(\lambda k_f)=-0.8$ changes Eq. (6) into Eq. (8).

In order to see how this behavior of $A_{max,min}$ is related to the bifurcation presented in Fig. 2 (solid curve), we plot in Fig. 4 $y=g(X)$ and $y=-A_{max,min}$ for $\lambda k_f=1$, 1.72, 1.722, and 4. The intersections between the curve $y=g(X)$ and the straight lines $y=-A_{max}$ and $y=-A_{min}$ show the (possible) boundaries of oscillations and from Fig. 1 we show the amplitude of stationary oscillation for $A=0.8$ by bold lines. This precisely reproduces the solid curve in Fig. 2 as is discussed below.

When $\lambda k_f$ is small [Fig. 4(a)], $A_{max}\simeq -A_{min}$ and from the first remark above we have $A'_{max}=A_{max}$ and $A'_{min}=A_{min}$. Thus we have two small amplitude oscillations, one around $x=1$ and the other around $x=-1$ (not shown), which is nearly symmetric with respect to $y$ axis in Fig. 4(a).

As $\lambda k_f$ approaches the critical point from below, $A_{min}$ increases rapidly as shown in the inset of Fig. 3. For example, at $\lambda k_f=1.72$ [Fig. 4(b)], $A_{max}=0.798$ and $A_{min}=-0.136$. Two curves $y=-A_{max}=-0.798$ and $y=g(x)$ has one intersection and this gives one large nonlinear oscillation corresponding to Fig. 1(b). Of course we have another solution with $A'_{max}=-A_{min}=0.136$ and $A'_{min}=-A_{max}=-0.796$, which gives large amplitude oscillatory solution in the region $-1<x_{f,p}(t)<0$ (not shown). This is symmetric, from the second remark above, with respect to $y$ axis in Fig. 4(b).

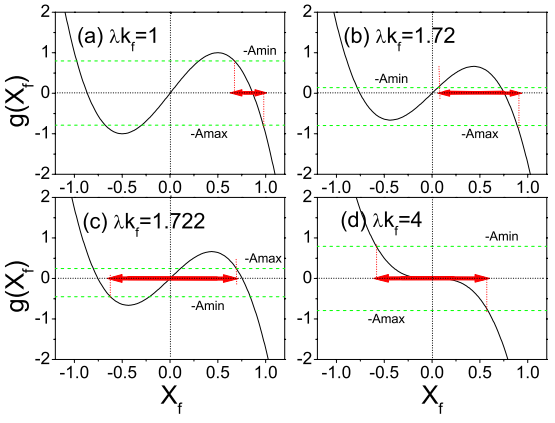


FIG. 4. (Color online) How the oscillation amplitude $Z(\lambda k_f)$ depends on the parameter $\lambda k_f$ with $A=0.8$, based on Eq. (6), where the solid curve represents $y=g(X)$, the dashed lines $y=-A_{max,min}$, and the bold arrow the oscillation amplitude $Z(\lambda k_f)$. (a)–(d) denote the cases $\lambda k_f=1$, 1.72, 1.722, and 4, respectively.

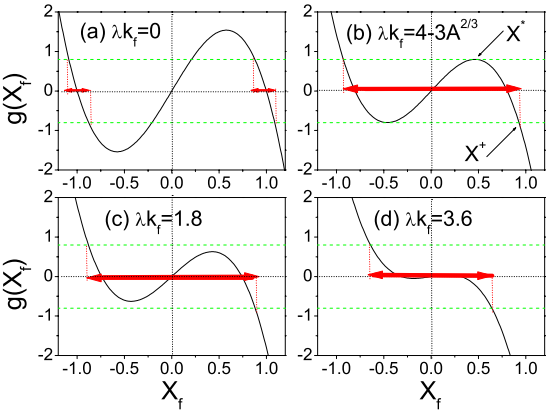


FIG. 5. (Color online) How the oscillation amplitude depends on the parameter $\lambda k_f$ with $A=0.8$ in the framework of Eq. (8), where the solid curve represents $y=g(X)$, the dashed lines $y=\pm A$, and the bold arrow the oscillation amplitude. (a)–(d) denote the cases $\lambda k_f=0$, $4-3A^{2/3}$, 1.8, and 3.6, respectively.

At the critical point where $A_{max}=A_{min}\equiv A_c$, we numerically confirmed that two separate oscillations in the positive and negative $x$ regions merge to give rise to large amplitude oscillation in the region $-1<x<1$. Since $A'_{max}=A'_{min}=-A_c$, we have here still two oscillations as remarked before. As $\lambda k_f$ increases a little beyond the critical point, $A_{max}$ decreases rapidly (see the inset of Fig. 3). For example, at $\lambda k_f=1.722$ [Fig. 4(c)], we have $A_{max}=-0.243$ and $A_{min}=0.454$ and see that the unit, confined in the region $1>x>0$ in the precritical situation, now moves over the range $-1<x<1$ in this postcritical situation.

When $\lambda k_f$ further increase, $A_{max}$ and $A_{min}$ approach $A$ and $-A$, respectively and the amplitude decreases as shown in Fig. 2.

Now we proceed to our theory. First we note that as long as we rely on the numerical Runge-Kutta solution of Eq. (5) to know $A_{max}$,$A_{min}$ in Eq. (6), we cannot obtain an analytic result for $G$, Eq. (4). To circumvent this difficulty, we introduce a second approximation, in which we neglect $\lambda k_f$ dependence of $A_{max}$ and $A_{min}$ and consider

$$A_{max}=A, \quad A_{min}=-A, \tag{7}$$

in addition to the fifty-fifty approximation. As mentioned above, from Fig. 3, we see that Eq. (7) is valid for $\lambda k_f>0$ except for a small $\lambda k_f$ region around $\lambda k_f^c$. In view of the merit of enabling us to obtain an analytic expression for $G$, we now proceed to discuss the results of Eq. (7).

From Eqs. (5) and (7), we consider instead of Eq. (6)

$$g(X_f)\equiv -4X_f^3-(\lambda k_f-4)X_f=\pm A. \tag{8}$$

The dashed curve in Fig. 2 represents $Z(\lambda k_f)$ from Eq. (8). Obviously, it is similar to the solid line from Eq. (6). Figure 5 shows graphically how the amplitude of oscillation changes with $\lambda k_f$ for $A=0.8$, where the solid curve represents $y=g(X)$, the dashed lines $y=\pm A$, the bold arrow the oscillation amplitude, and (a)–(d) denote the cases $\lambda k_f=0$, $4-3A^{2/3}$, 1.8, and 3.6, respectively, where $4-3A^{2/3}$ represents

a critical value $\lambda k_f^c$, whose derivation will be given below in Eq. (10).

Different from the results from Eq. (6), here the amplitude of oscillation decreases monotonously with $\lambda k_f$ for $\lambda k_f \geq \lambda k_f^c \equiv 4-3A^{2/3}$, see Fig. 2 (dashed curve). In Fig. 5(a), we observe that there are 6 solutions to Eq. (8). From a physical ground there are two oscillatory motion, one around +1 and the other around −1, both with small amplitude $2a_f$ indicated by a line with arrows on the $x$ axis. As $\lambda k_f$ increases $a_f$ also increases slowly and at the critical point $\lambda k_f^c = 4-3A^{2/3}$, $X_f$ experiences a finite jump, see Fig. 5(b).

$k_f^c$ can be determined from Eq. (8) as follows. We define $X^*$ [see Fig. 5(b)], where two curves $y=g(X)$ and $y=A$ are tangent each other. From $dg(X)/dX|_{X^*}=0$ we have

$$X^* = \sqrt{(4-\lambda k_f^c)/12}. \tag{9}$$

Since $g(X^*)=A$ we obtain an important result

$$\lambda k_f^c = 4-3A^{2/3}, \quad k_L(\lambda,A) = k_f^c = (4-3A^{2/3})/\lambda, \tag{10}$$

where $k_L$ denotes the degree of the node of maximum amplitude $a_L$.

The value of $a_L$ is readily determined as follows. From Fig. 5(b), $g(X^+)=-A$ and we obtain $X^+=A^{1/3}$. That is, our unit performs large amplitude oscillation between $\pm X^+ = \pm A^{1/3}$, with $\pm X^+$ denoting the nondegenerate solutions to Eq. (8) at $\lambda k_f = \lambda k_f^c$ and this realizes the maximum amplitude

$$a_L = X^+ = A^{1/3}, \quad G = a_L/A = A^{-2/3}. \tag{11}$$

When $\lambda k_f$ is further increased $X_f$ now starts to decrease from the value in Eq. (11).

As the SF network has a broadly distributed degree $k$, Eq. (3), we can find a node with $k=k_L$ for a wide range of $\lambda$. This result is meaningful because it tells us that the signal response can be amplified for a wide range of coupling strength $\lambda$, which is necessary and significant for the application of a signal device. On the other hand, for very small $\lambda$ it happens that we can find no node with the degree $k_L$, Eq. (10), for a finite system and here effects of finite size of the system come into play. This point will be considered later.

To check the validity of the prediction Eq. (10), we do numerical simulations to obtain experimentally $G$ and $k_L$, by first constructing 100 different SF networks and then providing them with randomly chosen initial configurations $\{x_i(t=0)=\pm 1\}$ for each $\lambda$. Thus we obtain 100 $k_L$ for each $\lambda$, based on which we calculate the average $\langle k_L \rangle$ and its standard deviation $\delta k_L = \sqrt{\langle (k_L - \langle k_L \rangle)^2 \rangle}$.

We plot $\langle k_L \rangle$ and its error bar (i.e., standard deviation) as a function of the coupling strength $\lambda$ in Fig. 6, where the solid curve is obtained from Eq. (10). Figure 6(a) denotes the case $N=500$ and Fig. 6(b) the case $N=2000$. From Figs. 6(a) and 6(b) it is easy to see that the theoretical curves are well confirmed by the numerical simulations except the small $\lambda$ region, and their consistence in Fig. 6(b) with larger size is better than that in Fig. 6(a) with smaller size. Their inconsistence in the small $\lambda$ region comes from the finite size effect, which will be discussed in the next section.

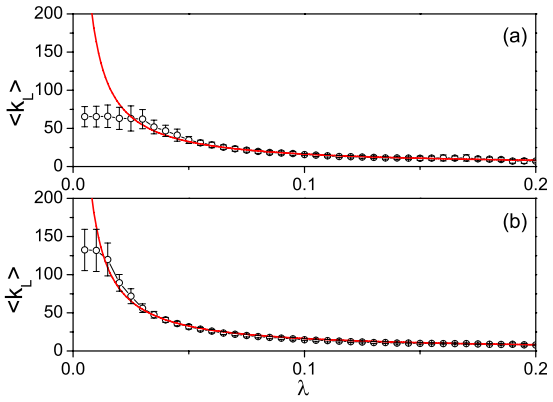


FIG. 6. (Color online) The average $\langle k_L \rangle$ and the standard deviation $\delta k_L$ of the degree of the unit L with maximum amplitude are shown by a circle and a bar as a function of $\lambda$, respectively. The solid curve is obtained from Eq. (10). (a) is for the case $N=500$ and (b) for the case $N=2000$. In simulations, we evaluated 100 $k_L$ for each $\lambda$, which are used to calculate $\langle k_L \rangle$ and $\delta k_l$.

The agreement between experiments and theory achieved for $k_L$ in Fig. 6 gives already a support to our fifty-fifty assumption. As a more direct check on this assumption, we calculated the ratio

$$r = \frac{n_+}{n_-}, \tag{12}$$

where $n_+$ ($n_-$) denotes the number of the neighbors which oscillate around +1(−1). It turned out that most of the $r$ from our experiments are around unity, confirming the fifty-fifty assumption.

## III. GAIN FOR THE WHOLE COUPLING RANGE

For a concrete network, an interesting question would be how its gain changes with the coupling strength $\lambda$. To answer this question, we divided the coupling range into three regions. The first region is $0<\lambda<\lambda_1$ with $\lambda_1$ satisfying $\lambda_1 k_{max} = 4-3A^{2/3}$, where $k_{max}$ denotes the largest degree of the concrete network at hand. The second region is $\lambda_1 < \lambda < \lambda_2$ with $\lambda_2$ being the point when the whole system begins to be synchronized. In the third region $\lambda > \lambda_2$ all the units oscillate with the same phase in the same well ($\pm 1$) as the input signal $A\sin(\omega t)$. From the above discussions our theory predicts that the gain for the second region is given by the formula Eq. (11), i.e., $G=A^{-2/3}$. Thus, in the following we will mainly focus on the first and third regions.

For the first region with $0<\lambda<\lambda_1$, no unit has a large enough degree $k$ to satisfy the relation Eq. (10) for $k_L$, which is revealed as the finite size effect in Fig. 6. Thus, all the units oscillate around their equilibriums, i.e., $\simeq \pm 1$. For a fixed coupling strength $\lambda$, the maximum amplitude of oscillation is expected to occur on the fifty-fifty unit. Let us put $k_f$ here be $k_{max}$. From Eq. (5) we easily obtain its solution

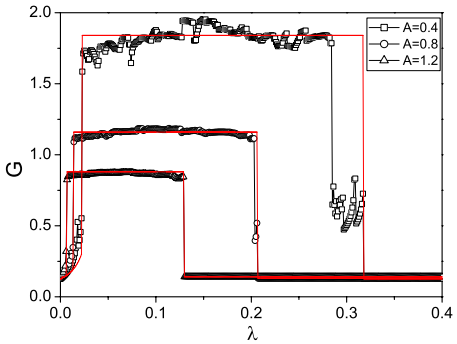


FIG. 7. (Color online) The gain $G$ as a function of the coupling strength $\lambda$ for a SF network with $N=2000$ and $\langle k\rangle=6$. From top, $A=0.4$, 0.8, and 1.2. Values of the gain in the middle "plateau" region are from the theory, Eq. (11), to be 1.84, 1.16, and 0.88, respectively for $A=0.4$, 0.8, and $A=1.2$ in good agreement with experiments.

$$x_f = x_0 + x_1(t), \tag{13}$$

where $x_0 = \pm\sqrt{\frac{4-\lambda k_{max}}{4}}$ is the equilibrium solution of Eq. (5) when there is no external force, and $x_1(t)$ is a linear response solution

$$x_1 = -\frac{A}{4(4-\lambda k_{max})^2+\omega^2}[\omega\cos\omega t - 2(4-\lambda k_{max})\sin\omega t]. \tag{14}$$

From $\dot{x}_f=0$ we can determine both $X_{max}$ and $X_{min}$ and obtain the gain $G \equiv (X_{max}-X_{min})/(2A)$ to be

$$G = \frac{1}{\sqrt{4(4-\lambda k_{max})^2+\omega^2}}. \tag{15}$$

As $\lambda k_{max} < 4-3A^{2/3}$ in this region, the gain $G$ will be small value and slowly increase from $1/\sqrt{64+\omega^2}$ to $1/\sqrt{36A^{4/3}+\omega^2}$ when $\lambda$ increases from 0 to $\lambda_1$.

For the third region with $\lambda > \lambda_2$, the dynamics is fully synchronized, $x_i(t)=x(t)(i=1,2,..,N)$. The Eq. (1) is reduced to

$$\dot{x} = -4x^3 + 4x + A\sin(\omega t). \tag{16}$$

Following the same argumentation employed to have Eq. (8) from Eq. (5), we have from Eq. (16)

$$-4X^3 + 4X = \pm A. \tag{17}$$

Denoting the solutions for $\pm A$ in Eq. (17) as $X_{max}$ and $X_{min}$, respectively, we have $a_{synch}=(X_{max}-X_{min})/2$, and thus $G_{synch}=a_{synch}/A$ is independent of $\lambda$ in this region. The solution to Eq. (17) can be also easily obtained graphically from Fig. 2 ($\lambda=0$).

We have thus obtained the gain $G$ for the whole range of coupling strength $\lambda$. For confirming it, we performed numerical simulations on a SF network with $N=2000$. Figure 7 shows the result for $A=0.4$ (squares), $A=0.8$ (circles), and $A=1.2$ (triangles).

In the first region $0<\lambda<\lambda_1$, we determine $\lambda_1$ from our theory $\lambda_1=(4-3A^{2/3})/k_{max}$ and the data $k_{max}\simeq 107$ to be $\lambda_1=0.022$, 0.013 and 0.006 for $A=0.4$, 0.8, and 1.2, respectively. The gain $G$ from Eq. (15) is plotted in the first region in Fig. 7(solid curves).

In the third region $\lambda>\lambda_2$, Eq. (17) is solved by the Newton-Raphson method [10] to obtain $G=0.126$, 0.131, and 0.141 for $A=0.4$, 0.8, and 1.2, respectively. As for $\lambda_2$ we have no reliable theory at the moment and they are determined from our numerical experiments as $\lambda_2=0.318$, 0.205, and 0.130 for $A=0.4$, 0.8, and 1.2, respectively.

At this point we give two comments on dynamics in the third region. First, in the synchronization processes we found from numerical experiments that nodes with large degree rather easily synchronize in the final attractive well (1 or −1), in contrast to nodes with small degree, which resist being attracted to the final well. Thus as a simple estimation of $\lambda_2$ we may put $k_L=5(7)$ in Eq. (10) to have $\lambda_2=0.47(0.34)$, 0.28(0.20), and 0.12(0.09) for $A=0.4$, 0.8, and 1.2, respectively. The estimation above based on the picture that synchronization as a whole starts when the most resistive unit synchronizes turns out to give at least qualitative prediction of $\lambda_2$.

Second, it is noted that for $\lambda\simeq 0.3(A=0.4)$, $G$ from experiments are observed to be larger than $G_{synch}$. Instead of attracted to the state of entirely synchronized state, the system seems to be trapped in a (meta)stable state, in which small number of units are oscillating in the well 1(−1) while all others in the well −1(1). For $A=1.2$ we observe no trace of metastability. To understand this phenomenon, we calculated $k_L$ at $\lambda=\lambda_2$ from Eq. (10) and obtain $k_L\simeq 7.6$, 6.8 and 4.7 for $A=0.4$, 0.8, and 1.2, respectively. This is in accord with the fact that when $k_L$ is relatively large it is easier to find some node with $k=k_L$ [see Eq. (3)]. From Fig. 6 it may be said that experimental results are reproduced by our simple one-body theory rather well.

## IV. DISCUSSIONS AND CONCLUSIONS

Different from the approach in [7], in this paper we developed a one-body theory for amplified signal response in a scale-free network. The concept of fifty-fifty unit made it possible to derive analytic forms for the gain, which consists of three approximate platforms. The existence of the middle platform shows that the SF network has the ability to amplify signal response in a broad range of coupling strength. Moreover, we reveal that the degree $k_L$ for the maximum amplification is inversely proportional to the coupling strength $\lambda$ and can be figured out by Eq. (10). All these results have been well confirmed by numerical simulations.

## ACKNOWLEDGMENT

One of the authors (T.M.) expresses his gratitude to Dr. M. Rosinberg for useful discussions at an early stage of this study.

[1] S. A. Langer and J. P. Sethna, Phys. Rev. Lett. **61**, 570 (1988); P. W. Anderson, B. I. Halperin, and C. M. Varma, Philos. Mag. **25**, 1 (1972).
[2] H. A. Kramers, Physica **7**, 284 (1940); N. G. Van Kampen, *Stochastic Processes in Physics and Chemistry* (Elsevier, Amsterdam, 1981), Chap. 13.
[3] R. Benzi, A. Sutera, and A. Vulpiani, J. Phys. A **14**, L453 (1981).
[4] L. Gammaitoni, P. Haenggi, P. Jung, and F. Marchesoni, Rev. Mod. Phys. **70**, 223 (1998).
[5] J. F. Lindner, B. K. Meadows, W. L. Ditto, M. E. Inchiosa, and A. R. Bulsara, Phys. Rev. Lett. **75**, 3 (1995).
[6] Z. Liu and T. Munakata, Phys. Rev. E **78**, 046111 (2008); F. Lu and Z. Liu, Chin. Phys. Lett. **26**, 040503 (2009); See also M. Perc, Phys. Rev. E **78**, 036105 (2008), where the periodic forcing is introduced to a single oscillator as a pacemaker.
[7] J. A. Acebron, S. Lozano, and A. Arenas, Phys. Rev. Lett. **99**, 128701 (2007).
[8] R. Albert and A. L. Barabasi, Rev. Mod. Phys. **74**, 47 (2002).
[9] A.-L. Barabasi and R. Albert, Science **286**, 509 (1999).
[10] W. H. Press, A. A. Teukolsky, and B. P. Flannery, *Numerical Recipes in C* (Cambridge University Press, Cambridge, England, 1988).